Available online at www.sciencedirect.com
SCIENCE DIRECT®
Journal of Power Sources 125 (2004) 256–266
JOURNAL OF POWER SOURCES
www.elsevier.com/locate/jpowsour

Electrolytic MnO_2 via non-isothermal electrode heating: a promising approach for optimizing performances of electroactive materials

M. Ghaemi*, R.K. Ghavami, L. Khosravi-Fard, M.Z. Kassaee

Department of Chemistry, School of Sciences, Tarbiat Modarres University, P.O. Box 14115-175, Tehran, Iran

Received 14 July 2003; accepted 28 July 2003

Abstract

A thermal-modulated electrodeposition technique is proposed for enhancing the physico-chemical characteristics of electrolytic manganese dioxide (EMD). Synthesis is conducted on the basis of non-isothermal electrode heating at ambient pressure. Electrode substrates are heated continuously during the anodic deposition processes in boiling sulfuric acid solutions. Bath temperatures and deposition parameters are held constant. Anode temperatures are varied in the range 98–150 °C. Two series of products, one deposited on a lead and the other on a Ti cylinder, are investigated. These are compared with EMD prepared by the conventional isothermal method which is similarly produced in a boiling solution. At optimized anode temperatures (120–135 °C), both series of products display enhanced charge–discharge performance. This is consistent with the compact surface morphologies which are obtained for thin layers of EMD deposited on graphite substrates.

The positive effects of localized heating are detected by electrochemical impedance spectroscopy. Several physico-chemical parameters of the solvent, as well as of the electrodes, are varied as a function of electrode temperatures. Conservation of energy can be obtained through a relatively safe, simple and low-cost process. This method has potential for application to other electroactive materials with industrial prospects.

Keywords: Non-isothermal electrodeposition; Electrode heating; Electrolytic manganese dioxide; Rechargeable alkaline manganese batteries

1. Introduction

Optimization of manufacturing parameters is of considerable interest for the development of advanced battery materials of high specific energy [1,2]. In this respect, many attempt have been made to lower energy consumption and processing cost by employing more efficient and innovative methods of synthesis. Many electrochemical aqueous systems suffer the disadvantage of not being able to be reduced or oxidized at temperatures below the boiling point of water. Nevertheless, several new radiation and thermal methods for the activation of electrochemical processes have emerged [3–7]. The ultimate solution appears to lie in finding a route to concentrate the thermal energy at the reaction surfaces. Perhaps the most favorable approach would be to concentrate the heat, in the thin hot solution layer, near the electrode surface [8]; as opposed to warming up the entire cell volume. While the idea may not be new, its principles have rarely been employed in electrosynthesis. The localized heating technique originally started with the pioneering work of Gründler et al. [9,10] who employed a contact technique called 'hot-wire electrochemistry'. This involves simultaneous heating of the working electrode with both alternating current and direct current. Such a technique allows a higher energy density to be localized in a small spot, near the working electrode. This activates those electrochemical processes which have slow charge-transfer kinetics at the lower temperature of the bulk solution. In addition, electrodeposition can be performed rapidly without waiting for warming up of the entire electrolyte solution. This saves both energy and time. Non-contact techniques with external heating (focused laser beam, microwave radiation, ultrasound, etc.) can also be used to heat electrode/electrolyte interfaces that have complex shapes [3,11]. The reaction zone may be heated to more than 373 K in an aqueous solution at atmospheric pressure and this may modify the electrocrystallization process [12].

A directly-heated electrode can be used to enhance the properties of electroactive materials, in particular those of semiconductors [13]. In this way, a stationary temper-

* Corresponding author. Tel.: +98-21-801-1001/3417; fax: +98-21-800-9730.
E-mail address: ghaemi_m@modares.ac.ir (M. Ghaemi).

0378-7753/$ – see front matter © 2003 Elsevier B.V. All rights reserved.
doi:10.1016/j.jpowsour.2003.08.036

ature both in and at the electrode surface is established. The temperature of the non-electrolytic backside and electrode/solution interface can be controlled very accurately. Electrochemical processes can be affected by changes in temperature-dependent parameters such as: heat induced convection, density, viscosity, electronic conductivity of the electrode substrate, volume expansion, and dielectric constant [14–18]. Therefore, the complex effects of temperature cannot be fully divorced from other variables of the system. In a broader sense, the growth mechanism incorporates the correlation of thermodynamics, kinetics, and transportation [19,20]. Two reports on the employment of directly- or indirectly-heated electrodes have been published [21,22]. The characteristics of non-isothermal electrode heating and its application to the electrosynthesis of electrolytic manganese dioxide (EMD) are discussed in the next section.

1.1. Characteristics of localized electrode heating

Generally, heat spreads much faster than changes in concentration. In contrast to conventional isothermal systems, a thermal boundary layer is established in non-isothermal systems and is quite similar to the concentration profile at the electrode. This causes the diffusion layer to be much thinner than the thermal layer [23]. Temperature differences inside the diffusion layer can be considered to be insignificant. Consequently, diffusion takes place at a temperature which is nearly uniform in the direction perpendicular to the electrode surface [4].

Increasing the temperature will increase the diffusion coefficients of generated as well as consumed species. In a non-isothermal system, not only diffusion but also convection can affect the electrochemical process. This is due to density gradients which are induced by a higher temperature at the electrode surface [24]. Both the increase in the rate of diffusion, as well as strong local boiling and stirring in the heated region of low viscosity, can contribute significantly to the enhanced ionic mass transport. This increases the rate of the electrodeposition process and the diffusion current, particularly in kinetically-controlled electrochemical reactions. Transport properties can be described by changes in the thickness of the diffusion layer (δ) and the diffusion coefficient (D) [14]. The difference in the limiting currents may well be described by the following:

$$\Delta i_l = nFAC\left[\frac{D_H}{\delta_H} - \frac{D_L}{\delta_L}\right] \quad (1)$$

The subscripts H and L designate the high and low temperatures of the electrode, respectively. In addition, due to the higher temperature in the synthesis zone than in the bulk a thermo-emf contributes to the applied potential [25,26]. This may bring about a current increase when working in a specific potential region.

The concentration of these electroactive materials, in the thin hot solution layer at the electrode surface, should be lower in comparison with the bulk. This may be due to the activation of a possible kinetically inhibited step and/or enhancement of transportation of species to/from the electrode surface. The increase in electrode temperature and the local heating is expected to have a strong influence on the nucleation and growth processes that are involved during deposition [11,27,28]. The grain size of the product generally increases with increase in temperature and results in denser packing of the solid product, with better electrical contact [20]. This could further prevent the access of other ions into the oxide.

At a higher electrode temperature, higher ion activity can be expected. At first, the hydrogen ion activity would be expected to increase as reflected by lower pH [20]. This is attributed to higher water dissociation at elevated temperatures. Since the hydrogen over potential has a negative temperature coefficient, it is worthwhile investigating the simultaneous employment of both a hot cathode and a hot anode in the electrodeposition process. However, this approach is not examined in this study.

1.2. Application of non-isothermal electrode heating on synthesis of electrolytic manganese dioxide

Manganese dioxide has long been studied for use in batteries [29–32]. The various manganese-based oxide frameworks may be classified into tunnel structures, layer phases, and spinels [33–39]. Electrolytic manganese dioxide is composed mainly of the polymorph γ-MnO_2 (mineralogically: nsutite) with random nano-sized microcavities and cracks. It involves De Wolff intergrowth structures of pyrolusite and ramsdellite polymorphs that contain water in different forms [40]. γ-MnO_2 crystals are not perfect and they are partly amorphous.

The electrochemical behavior of EMD, however, depends largely on the parameters of the anodic deposition processes. Several investigations focus on stabilizing manganese oxide structures against conversion into a pure electroactive spinel phase [33]. The electrochemical characteristics of EMD are improved through approaching the boiling point of electrolyte [41]. Bath temperatures, in the range of 95 °C to the boiling point of the electrolyte, are typically employed in the large-scale production of EMD. Since heating must be applied to the entire solution and evaporation loss is inevitable, these industrial methods of EMD production are economically less feasible.

As a possible alternative, temperatures above the boiling point of the electrolyte have been reached through an electrochemical-hydrothermal method using an autoclave [42]. The materials produced by this isothermal technique had a relatively higher degree of crystallinity and more desirable electrochemical performance in comparison with the traditional industrially prepared γ-MnO_2. Nevertheless, this method did not appear very safe nor economically sound for the production of EMD of high quality. It resulted in corrosion at high temperatures and required the employment of

high cost and complicated means to encounter related problems. Three years ago, interesting reports appeared on differential electrode heating, but without much detail [43,44]. Since then, no follow-up nor any elucidation of this procedure has appeared in the literature. Another parameter whose influence has frequently been neglected is utilization of the substrate temperature [45].

This study adopts a cost-effective route for the synthesis of EMD in a non-isothermal system and focuses on the effect of localized substrate heating on the electrocrystallization of EMD. The non-isothermal electrodeposition of EMD on various substrates at ambient pressure is reported. The performance characteristics of the EMD deposited at the heated electrode are examined. In addition, optimization of the reaction conditions and the experimentally determined limits of maximum heating of the electrode is demonstrated.

2. Experimental

2.1. Laboratory electrolyzer

A laboratory-scale plant shown in Fig. 1 was employed for the synthesis of EMD. In this plant, a cylindrical-shaped titanium or lead anode (65 mm inner diameter, 62 mm outer diameter, 125 mm long) was used as an electrolyte vessel. The vessel was immersed in electrically-heated silicon oil held at specific temperatures. A Teflon-coated magnetic stirrer served to circulate the oil. The cathode consisted of a porous lead tube (54 mm outer diameter) fixed into a spacer made of pyrex glass. Both electrodes were then connected to the contact wires by soldering.

Table 1
Electrodeposition conditions employed for synthesis of EMD

Anode substrate (electrolyte vessel)	Titanium, lead and graphite
Electrolyte composition	$MnSO_4$ 112 g l^{-1} in 0.10 M H_2S0_4 solution
Bath temperature	97–98 °C
Working electrode temperature	100, 120, 135 and 150 °C
Current density	$\leq$0.5 A dm^{-2}
Cell voltage	2.1–2.9 V (in all experiments)
Duration of electrolysis	72 h on titanium or lead, 10 min on graphite

2.2. Syntheses of EMDs and preparation of samples for SEM and EIS tests

Before each experiment, the Ti and Pb surfaces were mechanically polished with abrasive papers. All syntheses were performed in 330 ml boiling solutions of sulfuric acid which contained $MnSO_4$ (Table 1). EMD samples were prepared at substrate temperatures between 100 and 150 °C (Table 2). Electrolysis was carried out at a rather low current density to hold a lower value of the anodic overpotential. This is to avoid defective EMD structures caused by rapid growth at the electrode surface. All conditions were kept constant except for the substrate temperature. The precipitates obtained were removed mechanically from the anode and washed several times with distilled water. The products were then ground with a mortar and pestle and neutralized using 10% ammonia solution. Subsequently, the samples were dried at 80 °C overnight. The product was then filtered through a 100 μm mesh sieve in order to be used in rechargeable alkaline manganese (RAM) batteries. Since the surface morphologies of samples could be affected by various

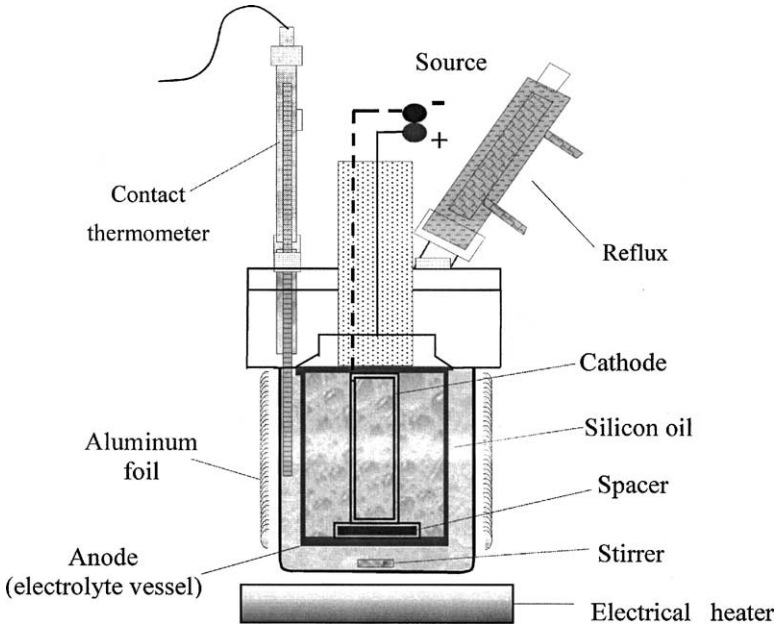

Fig. 1. Laboratory electrolyzer used for electrodeposition of manganese dioxide.

Table 2
Summary of all synthesized EMD samples along with their corresponding test batteries

EMD samples	Oil temperature (°C)	Electrode-substrates	Corresponding-batteries
Pb100	100	Pb	B-Pb100
Pb120	120	Pb	B-Pb120
Pb135	135	Pb	B-Pb135
Pb150	150	Pb	B-Pb150
Ti100	100	Ti	B-Ti100
Ti120	120	Ti	B-Ti120
Ti135	135	Ti	B-Ti135
Ti150	150	Ti	B-Ti150
G100	100	Graphite	–
G120	120	Graphite	–
G135	135	Graphite	–
G150	150	Graphite	–

parameters during electrolysis, short-time synthesis of EMD on graphite was performed under similar conditions for studying the effect of heat on thin-layer deposits.

Rectangular impregnated graphite (dimensions: 6 cm × 4 cm × 2 cm, type EK 2200 from SGL Carbon, Werk Ringsdorff, Bonn, Germany) was prepared with a wall thickness of 2 mm as the working electrode. The anode was placed inside a silicon oil bath maintained between 100 and 150 °C A Teflon-bonded reflux condenser was employed. Each experiment was performed for 10 min at a current density of $\leq$0.5 A dm^{-2} in a voltage range between 2.1 and 2.3 V (Tables 1 and 2). After electrolysis, the plated graphite was washed thoroughly with distilled water and immersed for 24 h in ammonia solution (pH: 8.5). Thereafter, all electrodes were cut into rectangular flat plates of 1 cm^2, weighed, and dried in the oven at 80 °C prior to use. The surface morphology of the grown films was investigated by scanning electron microscopy (SEM, Philips model XL 30).

Prior to electrochemical impedance spectroscopy (EIS) measurements discs of EMD electrodes were made. This was through mixing EMD powder (324 mg), graphite (Lonza KS44, 34 mg), acetylene black (2 mg) and adequate amounts of moisture followed by application of pressure at 6 ton cm^{-2} for 1 min. Impedance measurements were carried out in 9 M KOH, in a three-electrode cell, at ambient temperature, using an EG&G Parc potentiostat/galvanostat (model 273 A). Hg/HgO and a Pt wire were used as a reference and a counter electrode, respectively. A sinusoidal signal of 5 mV amplitude in a 100 kHz–0.01 Hz frequency interval was applied to the electrode at the open-circuit potential (OCV). Data acquisition was obtained using routine software (Zview 2.1).

2.3. Preparation of batteries

A laboratory-made RAM cell was assembled to determine the charge–discharge cycle performance of the different samples [42]. The cathode was prepared by mixing EMD with graphite, acetylene black, and polytetrafluorethylene (Table 3). This mixture was pressed at 6 ton cm^{-2} to form a cathode ring of 13 mm diameter with a thickness of an approximately 2 mm. The ring was put into a steel can which served as the cathode current-collector. Anode gel was prepared through mixing zinc with ZnO, MgO, α-cellulose, starch (Farinex 273) and an adequate amount of KOH (Table 2). The cycling characteristics were examined. This was to examine the effects of localized electrode heating on electrochemical performance. The electrochemical responses were measured using a computer connected to an in-house potentiostat–galvanostat. Charge–discharge cycling tests were carried out galvanostatically at a current density of 30 mA g^{-1} MnO_2 up to 15 cycles. All tests were conducted in a voltage range between a cut-off voltage (COV) of 0.9 and 1.72 V at room temperature.

Table 3
Cathode and anode composition used in laboratory RAM cells

Cathode composition	wt.%	Anode composition	wt.%
EMD	90	Zinc	61.5
Graphite	9.2	ZnO	3.4
Acetylene black	0.5	MgO	2.0
PTFE (polytetrafluorethylen)	0.3	α-Cellulose	1.0
		Starch (Farinex 273)	1.1
		KOH (12 normal)	31.0

3. Results and discussion

3.1. Temperature determination

Knowledge of the temperature at the electrode/solution interface is important for the interpretation of electrochemical phenomenon when a heated electrode is utilized [46]. Calculations are presented for determination of anode surface temperatures at Pb, Ti electrodes heated by external silicon oil. These surface temperatures are a function of the cell geometries and the heat-transfer coefficients of the electrode substrates [47]. The temperature gradient zone, between the electrode surface (T_s) and the electrolyte (T_f), lies within a thin layer of fluid adjacent to the electrode surface (Fig. 2). The heat transfer from the silicon oil, across the electrode to the electrolyte solution, takes place through heat conduction. The electrical energy power was 750–1000 W L^{-1} in both cases. The anode surface temperature (electrolyte site, T_f), for a multilayer (metal and MnO_2) cylinder with heat flow (q) to the metal surface (from T_s to T_f) is given by:

$$T_f = T_s - q\left(\frac{\sum\left(\frac{\ln(r_i)}{r_{i-1}}\right)}{2\pi k_i L}\right) \quad (2)$$

where T_f is the inner surface temperature; r_i the outer radius of the layer i; r_{i-1} the inner radius of the layer i; k_i the thermal conductivity of layer i; L is the length of the cylinder.

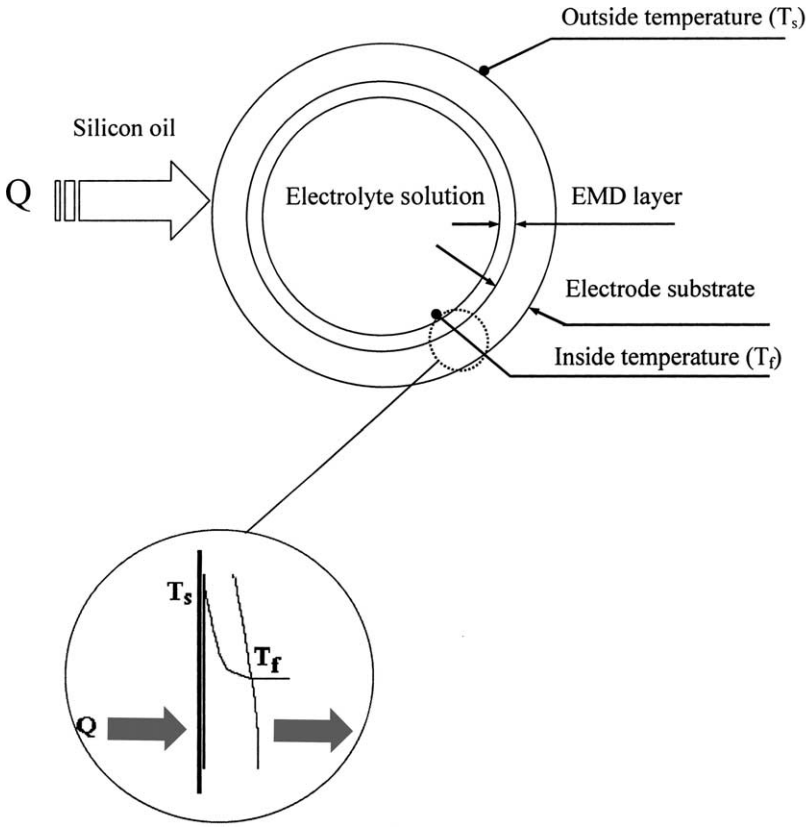

Fig. 2. Horizontal cross-section of electrolyzer used for electrodeposition of manganese dioxide (Fig. 1). Heat flow (Q) schematically illustrated as it transfers from the outer to the inner surface of the electrode (T_s vs. T_f). Enlargement in circle shows a thin boundary layer of electrolyte, adjacent to the electrode, where the main drop in temperature occurs.

Application of Eq. (3) allows evaluation of electrode surface temperatures independent of convection and other experimental parameters. These calculations are performed assuming similarity between pure water and the electrolyte solution as well as negligible influence of the deposited EMD layer on the heat transfer. The latter assumption is based on the low thickness of the variable EMD layer (approximately 0.15 mm at the end of synthesis). Calculated differences between the oil temperature (T_s) and the inner surface of the electrode (T_f) appear to be rather insignificant under the chosen experimental conditions.

3.2. Kinetics

Local superheating lowers the anodic overpotential but increases the heterogeneous charge-transfer kinetics. The thermal gradient, at the electrode/solution interface, controls the surface concentration of adsorbed intermediates. This could strongly affect chemical processes by lowering their activation energies to different degrees, as a function of their corresponding temperature coefficients [3]. Hence, one rate-controlling step may be replaced by another.

EMD is usually prepared by oxidative electrodeposition, from boiling acidic $MnSO_4$ solutions. The overall reaction for deposition of MnO_2 is given by:

$$Mn^{2+} + 2H_2O \rightarrow MnO_2 + 4H^+ + 2e^- \quad (3)$$

Paul and Cartwright [48] proposed a model for the electrochemical oxidation of Mn^{2+}, i.e.,

$$Mn(II) \rightarrow Mn(III) + e^- \quad (4)$$

$$Mn(III) + 2H_2O \rightarrow MnOOH + 3H^+ \quad (5)$$

$$MnOOH \rightarrow MnO_2 + H^+ + e^- \quad (6)$$

The rate of conversion of MnOOH to MnO_2 (Eq. (6)) is assumed to be slower in comparison with its rate of formation. Therefore, insulating porous layers of MnOOH are formed at the deposit surface and in structural defects. These passive layers retard the diffusion of manganese ions (Mn^{2+}) to the active sites of the electrode surface. The intermediate species are not able, however, to keep the surface in the passive state at higher temperatures. Such conditions may induce higher oxidation rates of intermediate MnOOH layers. This ultimately translates into a decrease of the thickness of these layers on the oxide surface. The number of MnOOH-free active sites increase, which makes reactions 4 and 5 proceed more readily.

Using pulse current for synthesis of EMD, an impairment of electrochemical cycle performance is observed as a reduction in the number of duty cycles [49]. Such a reduction makes MnOOH layers remain longer in the passive state. The lowering of the cycle performance, via approaching diffusional conditions, has negative effects on crystallinity. This approach is brought about by increasing the current density or decreasing the temperature and causes the EMD particles to lose contact with neighboring particles and the substrate. Under these conditions, reaction 4 occurs faster than the other steps (Eq. (4) ≫ Eqs. (5) and (6)). This is concurrent with decreasing mechanical strength and induces anodic overpotential.

The lower the synthetic temperature, the more is the probability for Mn^{3+} to diffuse into the solution and go through a disproportionation reaction to produce Mn^{4+} and Mn^{2+} (Eq. (7)) followed by formation of MnO_2 via hydrolysis of Mn^{4+} (Eq. (8)) [44].

$$2Mn^{3+} \rightarrow Mn^{2+} + Mn^{4+} \quad (7)$$

$$2Mn^{4+} + 2H_2O \rightarrow MnO_2 + 4H^+ \quad (8)$$

Manganese dioxide is formed and appears as a brown suspension in the solution. These reactions Eqs. (7) and (8) are, however, expected to occur at lower oxidation temperatures than those employed in this study. This hypothesis appears consistent with the experimental observations.

3.3. Cycle performance

The effects of changing Ti electrode temperatures (98–150 °C) on discharge capacities, as a function of cycle number, as well as cumulative capacities, are illustrated in Figs. 3 and 4, respectively. The same effects for a Pb electrode are demonstrated in Figs. 5 and 6. Interestingly, the

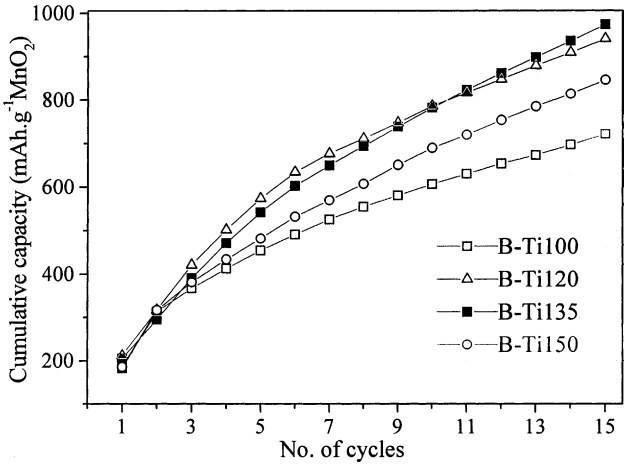

Fig. 4. Cumulative capacities of test batteries extracted from Fig. 3.

cycle performances for both electrodes appear to be highest in the range of 120–135 °C (Figs. 4 and 6). For both electrodes, cumulative capacities are higher for all substrate temperatures above the boiling point of the electrolyte solution (∼98 °C).

When Ti or Pb is employed as the electrode substrate, the formation of TiO_2 or PbO_2 is expected, respectively. A comparison capacities as a function of electrode temperature at 120 and 135 °C for Ti (Fig. 4) and Pb (Fig. 6) shows a better anchoring of deposits and more efficiency of heat transfer for Ti than for Pb. As a result, better charge–discharge cycling performances are observed for EMD deposited on Ti than on Pb at all temperatures (Fig. 7). Cumulative capacities fall at 150 °C (compared with 135 °C) when either Ti or Pb is employed as a substrate. Such observations may, at first, appear unexpected. These can be associated with the natural increase of the PbO_2 or TiO_2 thickness at 150 °C

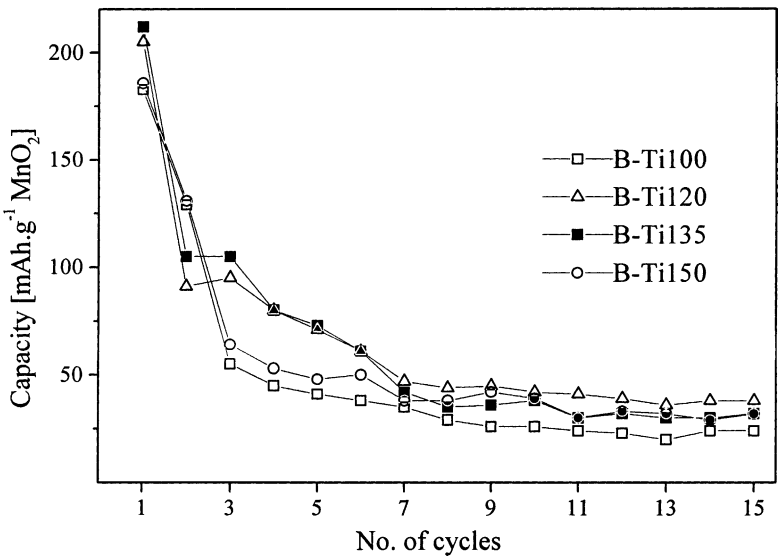

Fig. 3. Discharge capacities of RAM batteries for EMD samples deposited on Ti at 100 °C (B-Ti100), 120 °C (B-Ti120), 135 °C (B-Ti135) and 150 °C (B-Ti150). A cycle consists of discharge with 30 mA g^{-1} MnO_2 to a COV of 900 mV, followed by charge at 30 mA g^{-1} MnO_2 to a voltage limit of 1.72 V.

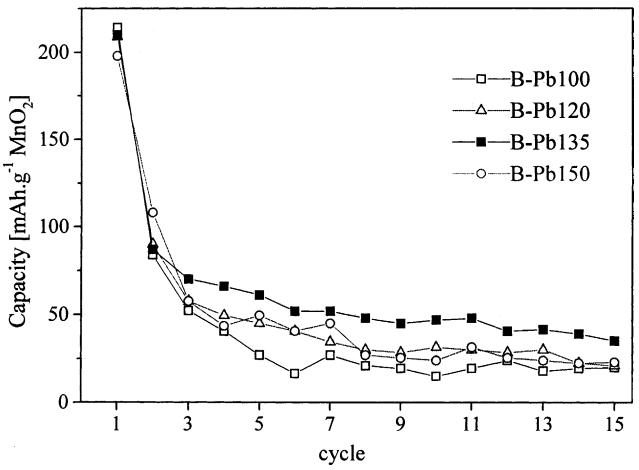

Fig. 5. Discharge capacities of RAM batteries for EMD samples deposited on Pb at 100 °C (B-Pb100), 120 °C (B-Pb120), 135 °C (B-Pb135) and 150 °C (B-Pb150). A cycle consists of discharge with 30 mA g^{-1} MnO_2 to a COV of 900 mV, followed by charge at 30 mA g^{-1} MnO_2 to a voltage limit of 1.72 V.

being more than at 135 °C, which results in an increase in the electric resistance in the bulk of the electrode.

Second, consideration should be given to the possibility of physical inflation of $Ti|TiO_2|MnO_2$ or $Pb|PbO_2|MnO_2$ layers as a function of the thermal expansion coefficients of corresponding layers. Obviously, such inflation at 150 °C reaches and/or surpasses the threshold level, where the inflation of layers ($Ti|TiO_2|MnO_2$ as well as $Pb|PbO_2|MnO_2$) produces sufficient stress and volume expansions (between these layers) to the extend of partial disruption of adhesion between the layers and the substrate. Hence, the stress at 150 °C becomes so large that heat transport becomes interrupted during the course of electrolysis. This lowers electrical contact, increases resistance, and increases anodic overpotential. A return to a usual anodic deposition may take place at a lower solution temperature. In such a case, the investigation may be conducted to heat a thin layer

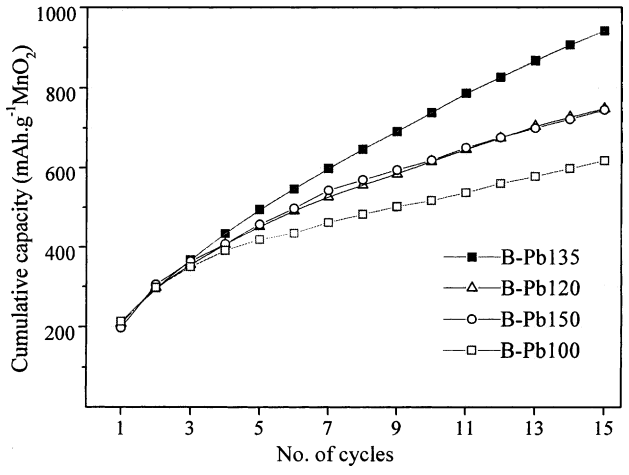

Fig. 6. Cumulative capacities of test batteries extracted from Fig. 5.

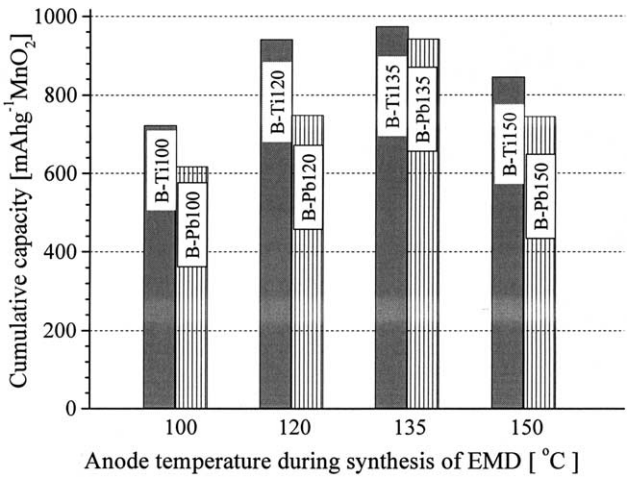

Fig. 7. Comparison of cumulative capacities of EMD samples produced on Ti and Pb.

solution near the electrode instead of heating the entire electrode. In this case, the substrate temperature remains below the lower bath temperature and prevents or slows down the formation of the oxide layers. Further studies are necessary to clarify the temperature dependence properties of various substrates.

3.4. Influence of bubbling, boiling and thermal-induced convection on EMD

EMDs deposited on graphite at 100 °C (G100), 120 °C (G120), 135 °C (G135) and 150 °C (G150) were compared and examined by means of SEM (Fig. 8(a)–(d)). An electron micrograph of G100 shows an irregular morphology with large cavities within fine, fragile thin layers (Fig. 8(a)). Scattered particle appear on the surfaces of these broken layers and do not have much internal cohesions. These particles tend to aggregate with increasing electrode temperature. Thus very few scattered particles are observed in G120, G135 and 150 (Fig. 8(b)–(d), respectively). Surface morphologies of deposited layers show no negative influence of bubbling, on the electrochemical cycle performance of EMD up to 135 °C. These pictures also show a decrease in the number of cavities as the electrode temperature is increased. Nevertheless, the relatively denser packing of EMD particles appears to increase up to 135 °C and decreases at 150 °C. In the case G150, mechanical detenoration through possible peeling of the deposit appears most pronounced at 150 °C (Fig. 8(d)). This may well be due to stronger bubbling of the solution and/or increase in oxygen evolution efficiency at this temperature. The increasing trend of interlayer spaces appear to be: G150 > G100 > G120 > G135.

An increase in capacity from G100 through G135 can mostly be related to the increase of electrode temperature. A similar effect was reported for a temperature increase of the electrolyte solution up to the boiling point [50,51]. Again, enlargement and swelling of the layers upon conglomeration

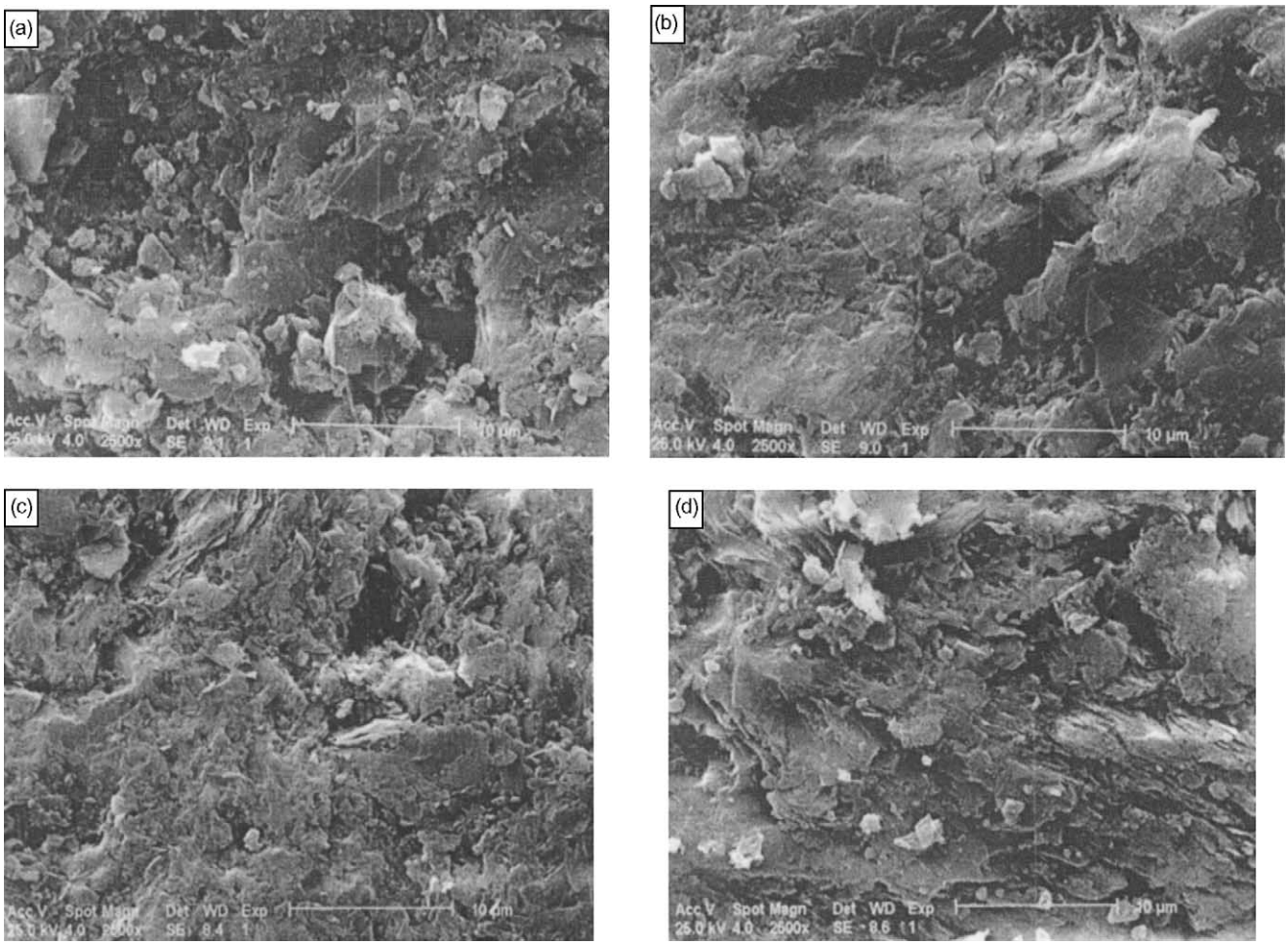

Fig. 8. Electron micrographs of (a) surface of G100: thin layer of EMD deposited on graphite at 100 °C; (b) surface of G120: thin layer of EMD deposited on graphite at 120 °C; (c) surface of G135: thin layer of EMD deposited on graphite at 135 °C; and (d) surface of G150: thin layer of EMD deposited on graphite at 150 °C.

is observed as a function of increasing electrode temperature from G135 to G150, and shows noticeable peeling at the latter temperature (Fig. 8(d)). This phenomenon may be held responsible for the possible increase of oxygen incorporation as well as the overvoltage of EMD at 150 °C. As a result, a reduction in the mechanical strength and a distortion of the crystal lattice occurs at this temperature.

Mechanical separation of deposited materials from both Pb and Ti substrates was undertaken with a steel hammer. The ease of such removal, for both substrates, appears to have the same trend, namely, 100 > 150 > 120 > 135 °C. These observations are consistent with cycle performance measurements (Figs. 4 and 6) and SEM morphologies (Figs. 8(a)–(d)).

While bubbling appears to have an effect on the EMD morphology at G150, boiling of the solution is speculated to have no influence on EMD characteristics in the temperature range employed. This speculation is mostly based on a report [52] in which the electrochemical behavior of EMD samples obtained prior to boiling (90 °C) is claimed to be similar to that recorded at the boiling point of the solution (97 °C). In the present preliminary tests, advantage was taken of this hypothesis in conservation of energy via keeping the solution in the cell below its boiling point. This was obtained either by passing a cold fluid through the solution or by circulating the electrolyte itself [53]. The finding have been sufficiently encouraging to take this approach further with results which will be presented in a latter communication.

The non-isothermal electrodeposition may be realized favorably in a non-boiling solution, so that the solution temperature remains lower than its boiling point. This is because of the energy consumption for evaporation and the restricted rate of nucleation for bubble formation [54]. Data presented in this study are somewhat consistent with previous results obtained in an autoclave (isothermal heating of the whole system without any heat-induced convection) [36]. Therefore, it can be concluded that there is no positive influence of thermal-induced convections on the cycle performance of MnO_2. This shows that mass transfer does not control the above oxidation process.

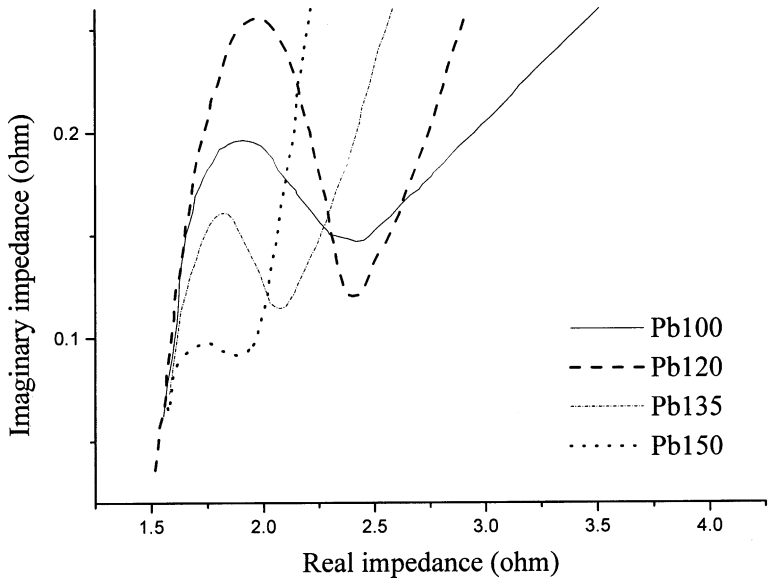

Fig. 9. Nyquist plots for cathodes with different EMDs deposited at various Pb substrate temperatures.

3.5. Interpretation of cycle performance via electrochemical impedance spectroscopy

Nyquist diagrams for EMDs deposited on Pb at 100–150 °C (Pb100 to Pb150) are presented in Fig. 9. The observed semicircles are formed through parallel combination of charge-transfer resistance (R_{ct}) and double-layer capacitance (C_{dl}). At lower frequency regions, these semicircles take linear shapes with different slopes, which indicates the extent of the diffusion-controlled processes involved. Having R_{ct} (Fig. 9), the value of C_{dl} can be calculated through [55]:

$$C_{dl} = \frac{1}{2\pi f' R_{ct}} \tag{9}$$

where f', is the frequency which corresponds to the maximum value of the imaginary component of the semicircle.

The effects of increasing Pb and Ti substrate temperatures on R_{ct} appear to have similar negative slopes with rather good correlation coefficients. This indicates the insensitivity towards the nature of the substrate (Fig. 10). The same conclusions are drawn for the effects of the increasing

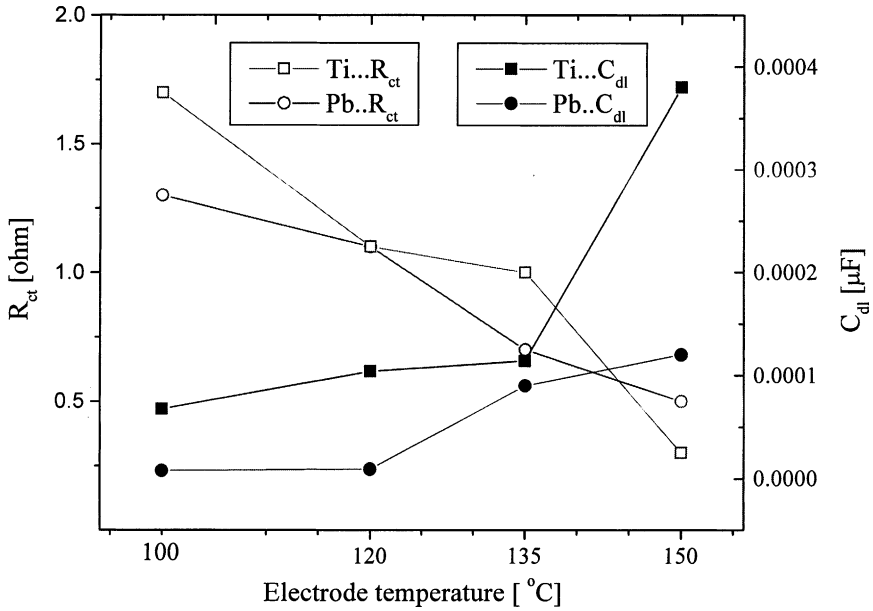

Fig. 10. Comparison of charge-transfer resistance (R_{ct}) and double-layer capacitance (C_{dl}) for cathodes with different EMDs deposited at various Pb and Ti substrate temperatures.

temperature of Pb and Ti substrates on C_{dl}. Positive slopes, obtained for both cases, indicate a high influence of electrode temperature on changes of C_{dl}, regardless of the nature of substrate.

Since all conditions in the working electrode have been kept constant; all measured parameters have been rightly related to properties of EMD as a function of direct and indirect effects of fabrication temperature. C_{dl} has been found to be proportional to the electrochemically accessible surface area of the EMD [56], which increased as a function of electrode temperature.

Even though the cycle performance declines at a lower synthesis temperature of 100 °C (Pb100 and Ti100) as well as at a higher temperature of 150 °C (Pb150 and Ti150), a different mechanism is speculated for each case. For Pb100 and Ti100, lower microporosity and/or insufficient current distribution can be expected [57,58]. These may induce local overdischarge with the production of excess Mn^{3+} ions, which facilitates Jahn-Teller lattice distortions [59]. The lower cycle performance can also be attributed to lower mechanical strength and/or disintegration of the EMD lattice in the cathode, due to the periodic dilations and contractions that accompany proton and electron transfer into and out of the lattice [60], i.e.,

$$MnO_2 + \delta H^+ + \delta e^- = H_\delta Mn_\delta^{III} Mn_{1-\delta}^{IV} O_2 \quad (10)$$

In addition, volume expansion of the cathode, due to the discharge process, may seal up those pores with small openings, and thereby reduce the active surface area of EMD. Hence, mass transfer in and out of these pores becomes more difficult during cycling.

Electrochemically accessible surface areas for Pb135, Ti135 and Ti120 are presumably less affected during cycling via higher synthesis temperatures than samples produced at 100 or 150 °C. This could be due to strengthening of the EMD, lattice at these temperatures, thus altering surface morphologies so that penetration of the ions is slowed down during synthesis and cycling (Fig. 8(a)–(c)). It could be expected that higher localized electrode heating within the EMD, as an n-type semiconductor electrode, is beneficial to reduce the *iR* drop at this inner resistance [61].

The decrease in the cycle performance of Pb150 and Ti150 may be related to the formation of cracks on the surface of the EMD (Fig. 8(d)). This could facilitate the incorporation and adsorption processes of other ions into the EMD lattice, and thus cause capacity fading during charge–discharge cycling [62].

The quality of EMD is improved through lowering of R_{ct}, as a function of substrate temperature [56]. Stability of the structural characteristics, especially the microporosity, appears to have a more dominating effect on rechargeability than either R_{ct} and/or C_{dl}, per se.

The characteristics of the microporous structure inside the manganese dioxide particles is mainly responsible for the charge-transfer process between the electrolyte and the crystal phase, the electrical conductance, and the transport properties of the crystal lattice. This behavior is due to a transport phenomenon which involves electrolyte diffusion inside the matrix of the porous electrode as well as proton transfer in the lattice of EMD. Proton transfer is affected by De Wolf disorder, micro-twinning and the crystal size/grain boundary as a function of electrode temperature [56]. Other temperature-dependent parameters such as the escape of lattice water during synthesis at 150 °C [63,64], adsorption of SO_4^{2-} during synthesis (not removed by washing), and cation and oxygen vacancies [65,66] could also affect the conductivity and electrochemical behavior. Further investigations, especially chemical analysis is required to clarify these considerations.

4. Conclusions

A non-isothermal electrode heating method is reported for the preparation of EMD and appears to be superior to conventional bulk heating as well as the electrochemical-hydrothermal synthetic route. Its advantages include higher charge–discharge cycle performance through possible increase in mechanical strength, current distribution, and/or conductivity. The method is relatively new, safe, simple, inexpensive and energy efficient, as well as being easily performable under mild conditions. A rise in temperature at the surface and inside the substrate can be achieved within a short time, without any need to heat the entire solution. This method is an effective means for activating the passive intermediates, including MnOOH.

Electrode heating does not appear to have a linear influence on cycle performance. It reaches a threshold maximum around 135 °C, when either Pb or Ti substrates are employed. Similarities between cumulative capacities obtained through isothermal (autoclave) and non-isothermal (anode heating) methods rule out the expected role of heat-induced convection in the latter method, and therefore gives more weight to the role of heat in both cases. The prospects of applying electrode heating to heterogeneous electrochemical processes with slow kinetics are under investigation.

Acknowledgements

The authors are grateful to Jaber Neshati from the Iranian Research Institute of Petroleum Industry for assistance with the EIS measurements.

References

[1] K. Shindo, M. Arakawa, T. Hirai, J. Power Sources 110 (2002) 46.
[2] A. Manthiram, J. Kim, Chem. Mater. 10 (1998) 2895.
[3] Y. Tsai, B.A. Coles, R.G. Compton, F. Marken, J. Am. Chem. Soc. 124 (2002) 9784.
[4] A. Beckmann, B.A. Coles, R.O. Compton, P. Gründler, F. Marken, A. Neudeck, J. Phys. Chem. B 104 (2000) 764.

[5] R.P. Akkermans, S.L. Roberts, F. Marken, B.A. Coles, S.J. Wilkins, J.A. Cooper, K.E. Woodhouse, R.G. Compton, J. Phys. Chem. B 103 (1999) 9987.
[6] D.D. Tuschel, J.E. Pemberton, Langmuir 4 (1988) 58.
[7] N. Sakamoto, T. Inoue, K. Kato, Cryst. Growth Des. 3 (2) (2003) 115.
[8] P. Gündler, Fresenius, J. Anal. Chem. 362 (1998) 180.
[9] P. Gründler, T. Zerihun, A. Kirbs, H. Grabow, Anal. Chim. Acta 305 (1995) 232.
[10] P. Gründler, A. Kirbs, T. Zerihun, Analyst 121 (1996) 1805.
[11] I. Zouari, F. Lapicque, M. Calvo, M. Cabrera, Chem. Eng. Sci. 45 (8) (1990) 2467.
[12] M. Okido, K. Kuroda, M. Ishikawa, R. Ichino, O. Takai, Solid State Ionics 151 (2002) 47.
[13] A.G. Muňoz, M.M. Lohrengel, J. Solid State Electrochem. 6 (2002) 513.
[14] J. Wang, M. Jasinksi, G. Flechsig, P. Gründler, B. Tian, Talanta 50 (2000) 1205.
[15] D.R. Lide (Ed.), Handbook of Chemistry and Physics, 82nd ed., CRC Press, Cleveland, OH, USA, 2001–2002, p. 6-3.
[16] K.J. Euler, H.M. Hesla, J. Power Sources 4 (1979) 77.
[17] M. Morita, C. Iwakura, H. Tamura, Electrochim. Acta 22 (1977) 325.
[18] K. Prabakar, S.K. Narayandass, D. Mangalaraj, Mater. Chem. Phys. 78 (2003) 809.
[19] N. Hackerman, Ind. Eng. Chem. 44 (8) (1952) 1752.
[20] S. Seif, J.M. Chang, K. Bhat, B. Penn, R.B. Lal, Cryst. Growth Des. 1 (5) (2001) 359.
[21] J. Wang, P. Gründler, O. Flechsiga, M. Jasinski, J. Lua, J. Wang, Z. Zhao, B. Tian, Anal. Chim. Acta 396 (1999) 33.
[22] S.L. Brock, N. Duan, Z.R. Tian, O. Giraldo, H. Zhou, S.L. Suib, Chem. Mater. 10 (1998) 2619.
[23] F. Qiu, R.G. Compton, B.A. Coles, F. Marken, J. Electroanal. Chem. 492 (2000) 150.
[24] T. Voss, P. Gründler, C.M.A. Brett, A.M.O. Brett, J. Pharma. Biochem. Anal. 19 (1999) 127.
[25] A.S. Baranski, Anal. Chem. 74 (2002) 1294.
[26] V.A. Benderskii, G.I. Velichko, J. Electroanal. Chem. 140 (1982) 1.
[27] H. Harada, N. Yoshida, K. Yamamoto, T. Itoh, K. Inagaki, H. Inouchi, N. Yamana, T. Aoki, S. Nonomural, S. Nitta, Solar Energy Mater. Solar Cells 66 (2001) 253.
[28] H. Ma, J.S. Cho, C.H. Park, Surf. Coat. Technol. 153 (2002) 131.
[29] K.V. Kordesch, US Patent 3,288,642 (1966).
[30] K.V. Kordesch, A. Kozawa, US Patent 3,945,847 (1976).
[31] L. Binder, W. Odar, K.V. Kordesch, J. Power Sources 6 (1981) 271.
[32] L. Binder, W. Jantscher, F. Hofer, G. Kothleitner, J. Power Sources 70 (1998) 1.
[33] M.S. Whittingham, P.Y. Zvalij, Solid State Ionics 131 (2000) 109.
[34] M.V. Ananth, S. Pethkar, K. Dakshinamurthi, J. Power Sources 75 (1998) 278.
[35] W. Jantscher, L.D.A. Fiedler, R. Andreaus, K.V. Kordesch, J. Power Sources 79 (1999) 18.
[36] S. Sarciaux, A. Le Gal La Salle, A. Verbaere, Y. Piffard, D. Guyomard, J. Power Sources 81–82 (1999) 656.
[37] P. Lavela, L. Sànchez, J.L. Tirado, S. Bach, J.P. Pereira-Ramos, J. Power Sources 84 (1999) 75.
[38] S. Bodoardo, N. Penazzi, P. Spinelli, M. Arrabito, J. Power Sources 94 (2001) 194.
[39] M.M. Sharma, B. Krishnan, S. Zachariah, C.U. Shah, J. Power Sources 79 (1999) 69.
[40] S.W. Donne, F.H. Feddrix, R. Glöckner, S. Marion, T. Norby, Solid State Ionics 152–153 (2002) 660.
[41] G. Pistoia, J. Electrochem. Soc. 129 (1982) 1861.
[42] M. Ghaemi, Z. Biglari, L. Binder, J. Power Sources 102 (2001) 29.
[43] A.G. Kholmogorov, A.M. Zhyzhaev, U.S. Kononov, G.A. Moiseeva, G.L. Pashkov, Hydrometallurgy 56 (2000) 1.
[44] V.V. Patrushev, Y.S. Kononov, G.L. Pashkov, RU Patent 2115769 (1996).
[45] P. Van Daele, D. Lootens, P. Demeester, Vacuum 41 (4–6) (1990) 906.
[46] T. Zerihun, P. Gründler, J. Electroanal. Chem. 404 (1996) 243.
[47] http://www.mayahtt.com/tmwiz/default.htm.
[48] Z. Rogulski, H. Siwek, I. Paleska, A. Czerwiński, J. Electroanal. Chem. 543 (2003) 175.
[49] M. Ghaemi, L. Binder, J. Power Sources 111 (2002) 248.
[50] B. Preisler, Electrochim. Acta 26 (10) (1981) 1389.
[51] M. Ghaemi, Dissertation, Technical University of Graz, Austria 1995.
[52] A. Le Gal La Salle, S. Sarciaux, A. Verbaere, Y. Piffard, D. Guyomard, J. Electrochem. Soc. 147 (3) (2000) 945.
[53] L. Binder, M. Ghaemi, K.V. Kordesch, in: F. Lapicque, et al. (Eds.), Electrochemical Engineering and Energy, Plenum Press, New York, 1995, pp. 33–40.
[54] P. Gründler, D. Degenring, J. Electroanal. Chem. 512 (2001) 74.
[55] S. Rodrigues, N. Munichandraiah, A.K. Shukla, J. Power Sources 87 (2000) 12.
[56] D. Qu, J. Power Sources 102 (2001) 270.
[57] T. Våland, J. Power Sources 1 (1976) 65.
[58] K.-J. Euler, The Late Ulrich Euler, Burkhart Seim, J. Power Sources 6 (1981) 25.
[59] J.B. Fernandes, B.D. Desai, V.N. Kamat Dalal, J. Power Sources 15 (1985) 209.
[60] J.W. Long, K.E. Ayers, D.R. Rolison, J. Electroanal. Chem. 522 (2002) 58.
[61] L.M. Gassa, H.T. Mishima, B.A. Lopez de Mishima, J.R. Vilche, Electrochim. Acta 42 (1997) 1717.
[62] N. Hackerman, Ind. Eng. Chem. 44 (1952) 1752.
[63] R. Giovanoli, Thermochim. Acta 234 (1994) 303–313.
[64] M. Tsuda, H. Arai, Y. Sakurai, J. Power Source 110 (2002) 52.
[65] K. Matsuki, T. Endo, H. Kamada, Electrochim. Acta 30 (10) (1985) 1329.
[66] P. Ruetschi, J. Electrochem. Soc. 131 (1984) 2737.